Applied Physics A (2019) 125:801
https://doi.org/10.1007/s00339-019-3105-8

Applied Physics A
Materials Science & Processing

Assessment of nuclear shielding and alpha/proton mass stopping power properties of various metallic glasses

Ufuk Perişanoğlu[1]

Received: 27 September 2019 / Accepted: 25 October 2019 / Published online: 3 November 2019

Abstract
This work aimed to investigate alpha, proton, neutron and gamma shielding qualifications of different bulk metallic glasses ($Zr_{65}Al_{7.5}Ni_{10}Cu_{17.5}$, $Ti_{40}Zr_{26}Be_{28}Fe_6$, $Cu_{49}Hf_{42}Al_9$, $Pd_{40}Ni_{40}P_{20}$, $Ni_{50}Pd_{30}P_{20}$, and $Ca_{65}Mg_{15}Zn_{20}$) for nuclear security applications. Therefore, vital gamma radiation attenuation parameter namely mass attenuation coefficients (μ_ρ) of investigated bulk metallic glasses (BMG) were determined using WinXCOM program. Next, half value layer (HVL), effective atomic number (Z_{eff}), effective electron density (N_{el}) and exposure buildup factors (EBF) were perused in a wide energy interval (0.02–20 MeV). Among the investigated samples, MG3 was found to be superior attenuator sample for gamma radiation, while MG6 was the least forceful glasses to reduce the photon intensity. The elements Pd and Hf in MG4, MG5 and MG3 were enhanced radiation shielding competences of the BMGs. Further, fast neutron removal cross-sections ($\sum R$) were evaluated to investigate neutron protection ability of the BMGs. Projected range (PR) and mass stopping power (MSP) values were obtained for proton (H^{1}) and alpha particles (He^{+2}). The outcomes showed that elemental composition of the metallic glasses was highly powerful on alpha, proton and neutron attenuation. It can be concluded that MG3 sample exhibited high nuclear shielding efficiency as deduced from the largest μ_ρ, Z_{eff}, and $\sum R$, and the lowest HVL, EBF, MSP and PR values.

1 Introduction

The active use of radioactive sources in many areas of life has made essential the production of shielding materials to protect against the deleterious impacts of radiation. In this sense, researchers have carried out studies on many shielding materials such as concretes [1, 2], glasses [3, 4], and alloys [5]. Among the these material types, glasses have gained a major attention from researchers due to its physical and chemical properties such as ease of production, optical transparency, high corrosion resistance and eco-friendly [6]. Kavaz et al. [7–9] examined the physical, structural and gamma ray protection features of lithium borate glasses obtained by adding various minerals using different codes such as MCNPX and WinXCOM. Sayyed et al. [6, 10, 11] have reported many studies on the optical, structural and multiple nuclear radiation shielding features of various heavy metal-doped glass systems using WinXCOM software, GEANT4 and MCNPX simulation codes. Previously, Shams et al. surveyed the radiation shielding and mechanical properties of the TeO_2–ZnO–NiO, PbO–$Na_2B_4O_7$–CaO–Al_2O_3–SiO_2 and Al_2O_3–Na_2O–B_2O_3–Bi_2O_3 glass systems [12–14]. In all studies, it is seen that the use of heavy metal-containing oxides in glass synthesis increases density and nuclear radiation shielding ability of the material.

Amorphous alloys, i.e., metallic glasses, have been researched and developed about half a century ago. By adding new metals, many important properties of these glasses have been investigated for utilization in structural and functional applications. Previously, they were frangible and produced in micron thicknesses, which limited the application areas [15]. However, the studies led by a special working group in Japan [16–19] have overcome the problems in size and during production. Bulk metallic glasses own unique properties such as high toughness [20] and strength, good corrosion resistance [21], high elastic tensile, low internal friction and elastic modulus, good machinability, tensile strength up to 3000 MPa [22]. In addition, their superior performance against high temperature and pressure allows the use of these amorphous alloys in many industrial applications (industry, sports equipment, biomedicine and consumer electronics) [23].

✉ Ufuk Perişanoğlu
ufukperisanoglu@gmail.com

[1] Department of Physics, Faculty of Science, Ataturk University, 25240 Erzurum, Turkey

Given the fact that the production of new amorphous alloy systems and many of their properties can be modified depending on the metals used, metallic glasses are extremely attractive materials for technological applications and scientific research. In recent years, Inoue's works [17, 19, 24–26] have shown that the production of multicomponent bulk metallic glasses (BMG) which possess high-glass forming ability (GFA) could be produced. Many amorphous alloys such as ZrTiCuNiBe, TiNiCuSn, CuZrTiNi, NdFeCoAl, LaAlNi, FeCoNiZrNbB, FeAlGaPCB, PrCuNiAl, and PdNiCuP of 5–10-cm thickness were reported to be developed [15]. In the present century, BMGs are now regarded as the most sought materials in structural engineering due to their high mechanical properties [27]. Ion irradiation method is utilized for exploring the microstructure and mechanical properties of BMGs [28]. Information about their hardness, free volume and atomic structure can be obtained by methods such as X-ray diffraction and positron annihilation. Moreover, ion irradiation might also support to manufacture and use novel BMG for structural nuclear material under radiation medium [29].

In addition to the unique features mentioned in the above paragraphs BMGs with high density and both glass and alloy properties appear to be worth investigating for radiation protection studies. Due to the lack of studies on the shielding parameters of metallic glasses in the literature, the radiation shielding competences of NiPdP, CaMgZn, CuHfAl, ZrAlNiCu, PdNiP, and TiZrBeFe metallic glasses were surveyed in the current work. The main shielding parameter which is the mass attenuation coefficient (μ/ρ, cm^2/g) was found from the chemical compositions of six metallic glasses. From that parameter, effective atomic number (Z_{eff}), electron density (N_{el}), and half value layer (HVL) values of the BMGs were also calculated. Exposure buildup factor (EBF) values, another important gamma interaction parameter, were found for 1–40 mfp at 0.015–15 MeV photon energies by the Geometric Progression (GP)-fitting approach. Lastly, fast neutron removal cross-sections (Σ_R), projected range (PR) and mass stopping power (MSP) for alpha (He^{+2}) and proton (H^1) particles have been found for the particle shielding effectiveness of selected metallic glasses. It can be emphasized that the outcomes obtained from the current study will beneficial for future enforcements of different types of metallic glass in the sense of radiation shielding purposes.

Table 1 Sample codes, name and density of the bulk metallic glasses

Sample code	BMG	Density (g/cm^3)
MG1	$Zr_{65}Al_{7.5}Ni_{10}Cu_{17.5}$	6.78
MG2	$Ti_{40}Zr_{26}Be_{28}Fe_6$	4.48
MG3	$Cu_{49}Hf_{42}Al_9$	10.12
MG4	$Pd_{40}Ni_{40}P_{20}$	7.96
MG5	$Ni_{50}Pd_{30}P_{20}$	7.62
MG6	$Ca_{65}Mg_{15}Zn_{20}$	2.69

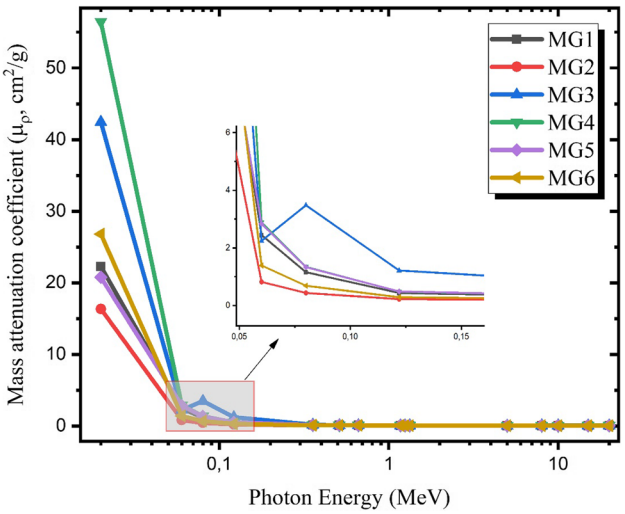

Fig. 1 The changes of mass attenuation coefficient of the BMGs with photon energy

2 Materials and methods

As gamma photons pass through a material of a thickness (x), the intensity of the photons is attenuated, and this attenuation is defined by Beer–Lambert's law [30]:

$$\mu = \ln(I_0/I)/x, \tag{1}$$

where the I and I_0 denote the incident and transmitted photon intensities and x refers the mass thickness of the irradiated material. μ refers the linear attenuation coefficient (cm^{-1}) of the sample and depends on the composition of the samples, the energy of the incident photon, the density and thickness of the sample. Another vital parameter which is the mass attenuation coefficient (μ_ρ, cm^2/g) is an indication of the ability of the material to attenuate against gamma radiation. By utilizing the weight fraction (w_i) of the ith component of a metallic glass sample, the μ_ρ can be calculated according to the formula [31]:

$$\mu_\rho = \sum_i w_i(\mu/\rho)_i. \tag{2}$$

The detection of μ_ρ values of the metallic glasses was acquired at 0.02–20 MeV gamma ray energies with using WinXCOM program [32].

Mean Free Path (MFP) is described as the average length of the path that a photon experiences successive interaction and MFP is given with next relation:

$$\text{MFP} = (1/\mu). \tag{3}$$

Table 2 The mass attenuation coefficient (μ_ρ, cm^2/g) of the metallic glasses

Energy (MeV)	MG1	MG2	MG3	MG4	MG5	MG6
0.02	22.285	16.342	42.438	56.441	20.769	26.800
0.06	2.445	0.818	2.242	2.884	2.834	1.390
0.08	1.156	0.434	3.479	1.340	1.331	0.685
0.122	0.434	0.221	1.213	0.484	0.487	0.288
0.356	0.109	0.102	0.152	0.108	0.111	0.098
0.511	0.087	0.087	0.102	0.085	0.087	0.081
0.662	0.075	0.077	0.082	0.073	0.075	0.071
1.173	0.056	0.058	0.056	0.054	0.055	0.054
1.25	0.054	0.056	0.054	0.052	0.054	0.052
1.33	0.052	0.054	0.052	0.051	0.052	0.050
5	0.033	0.031	0.035	0.033	0.033	0.029
8	0.032	0.029	0.036	0.033	0.032	0.027
10	0.032	0.028	0.037	0.033	0.033	0.027
15	0.034	0.028	0.040	0.036	0.035	0.027
20	0.036	0.029	0.043	0.038	0.037	0.028

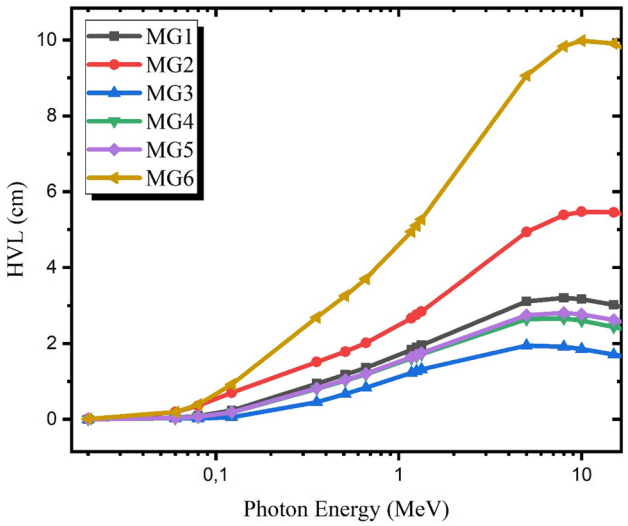

Fig. 2 HVL values of the metallic glasses

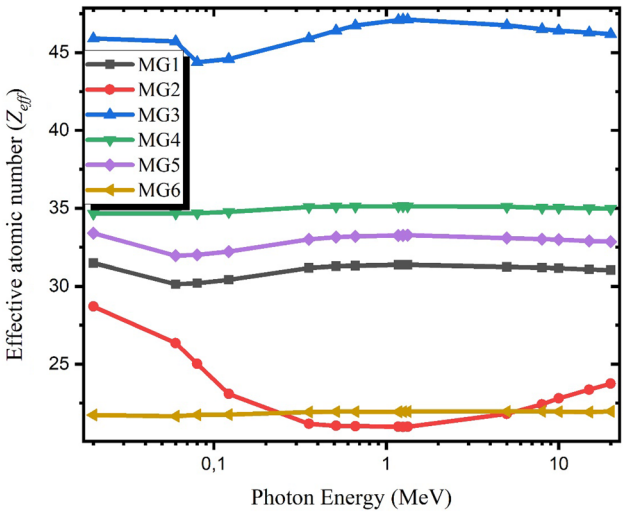

Fig. 3 Variations of Z_{eff} versus gamma energy for metallic glasses

Half value layer (HVL) is an advantageous variable for designing and choosing any photon reduction material because it demonstrates the thickness of the material necessary to attenuate the radiation level to 50% of its initial value and HVL is founded with the next equation [33]:

$$\mathrm{HVL} = (\ln 2/\mu). \tag{4}$$

The effective atomic number (Z_{eff}) is a handy variable for explaining the attenuation of gamma radiation in multi-element medium and ensures information about the target material. Effective atomic number (Z_{eff}) and effective electron density (N_{el}) of the metallic glasses were calculated according to the following relations:

$$Z_{\mathrm{eff}} = \frac{\sum_i f_i A_i (\mu_\rho)_i}{\sum_j f_j \frac{A_j}{Z_j} (\mu_\rho)_j} \tag{5}$$

$$N_{\mathrm{el}} = N_A \frac{Z_{\mathrm{eff}}}{\langle A \rangle} (\mathrm{electrons/g}). \tag{6}$$

To use a single atomic number in complex materials, an effective atomic number (Z_{eff}) is needed. By dividing Z_{eff} by the average atomic number, N_{el} is obtained, which is the number of electrons per unit mass.

Exposure buildup factor (EBF) depends on the energy absorption response of air and EBF is considered equivalent to the measured value of the dose absorbed in air by an

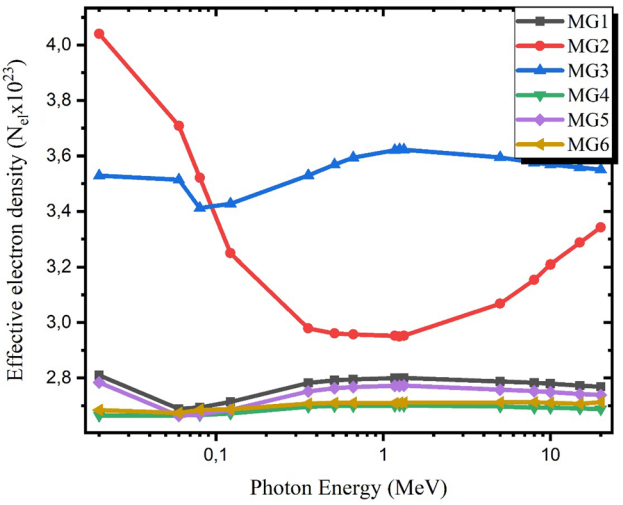

Fig. 4 Variations of N_{el} versus gamma energy for glasses

unperturbed detector. Basically, an equivalent atomic number (Z_{eq}) must be attributed to each material for the photon energies studied, when buildup factors are calculated for the chosen substance. Since the buildup factor chiefly arises from incoherent scattering, the Z_{eq} is computed employing the ratio of incoherent scattering to total attenuation with incoherent scattering [34]. Geometric Progression (GP) fitting coefficients were determined using an interpolation formula, with the calculation of equivalent atom numbers. GP fitting parameters are obtained from the standard reference database ANSI/ANS-6.4.3. Then, the GP fitting parameters are used exposure buildup factors from the GP fitting formula that has been repeatedly mentioned in previous publications [35–38]

The effective removal cross-section ($\sum R$) is the probability of one neutron undergoing a specific reaction passing across the BMG medium. To compute the sum of $\sum R$ of investigated samples, the next relation is used for each sample, respectively [1]:

$$\sum R = \sum W_i \left(\sum R/\rho \right)_i \tag{7}$$

where W_i and $\sum R/\rho$ refer the partial density(g/cm^3) and the mass removal cross-section (cm^2/g) of the *i*th element.

The mass stopping power (MSP) establishes how accomplished a material is in reducing the kinetic energy of the charged particles and projected range (PR) states the average range for stopping the charged particles. The very frequently employed method for finding stopping power and projected

Table 3 Equivalent atomic numbers of the metallic glasses for the energy range 0.015–15 MeV

Energy (MeV)	MG1	MG2	MG3	MG4	MG5	MG6
0.015	24.953	21.600	59.834	23.284	24.532	19.139
0.02	24.000	21.688	60.189	35.942	24.551	26.024
0.03	32.828	21.819	60.540	36.128	34.923	26.736
0.04	33.235	21.899	64.963	36.274	35.315	27.154
0.05	33.500	21.953	64.896	36.350	35.573	27.427
0.06	33.687	21.999	33.237	36.397	35.751	27.623
0.08	33.895	22.067	51.721	36.427	35.935	27.897
0.1	34.017	22.116	52.420	36.404	36.030	28.088
0.15	34.106	22.194	53.376	36.248	36.050	28.377
0.2	34.104	22.240	53.912	36.077	35.991	28.547
0.3	34.090	22.292	54.546	35.874	35.915	28.742
0.4	34.101	22.322	54.921	35.794	35.902	28.856
0.5	34.121	22.342	55.182	35.754	35.911	28.932
0.6	34.134	22.353	55.356	35.731	35.921	28.966
0.8	34.150	22.366	55.539	35.719	35.932	29.010
1	34.149	22.367	55.622	35.711	35.929	29.020
1.5	33.456	21.670	54.556	35.520	35.225	26.913
2	32.172	21.009	51.919	35.168	33.924	24.016
3	30.988	20.774	39.560	34.868	32.799	22.553
4	30.616	20.715	45.777	34.767	32.388	22.139
5	30.432	20.681	44.778	34.709	32.164	21.950
6	30.300	20.661	44.240	34.685	32.005	21.804
8	30.150	20.642	43.542	34.657	31.852	21.667
10	30.091	20.631	43.158	34.659	31.777	21.615
15	30.111	20.622	42.822	34.704	31.772	21.570

Table 4 The EBF GP fitting coefficients (b, c, a, X_k and d) of MG2 sample

E (MeV)	EBF				
	b	c	a	X_k	d
0.015	1.011	0.197	0.534	10.77	− 0.5094
0.020	1.012	0.130	0.621	11.39	− 0.619
0.030	1.026	0.370	0.194	24.88	− 0.2485
0.040	1.052	0.334	0.244	12.79	− 0.1096
0.050	1.085	0.359	0.238	13.45	− 0.1381
0.060	1.126	0.382	0.224	13.81	− 0.126
0.080	1.216	0.454	0.188	14.15	− 0.1052
0.100	1.317	0.522	0.159	13.95	− 0.0885
0.150	1.548	0.689	0.096	14.02	− 0.0539
0.200	1.717	0.847	0.049	13.56	− 0.0359
0.300	1.875	1.030	0.004	12.45	− 0.0196
0.400	1.914	1.139	− 0.019	11.40	− 0.0137
0.500	1.912	1.191	− 0.029	9.850	− 0.0105
0.600	1.888	1.214	− 0.035	8.570	− 0.0092
0.800	1.846	1.224	− 0.037	7.110	− 0.0118
1.000	1.815	1.203	− 0.034	7.530	− 0.0114
1.500	1.748	1.196	− 0.04	16.18	0.0110
2.000	1.721	1.132	− 0.024	11.28	− 0.0010
3.000	1.634	1.065	− 0.008	12.66	− 0.0097
4.000	1.566	1.016	0.006	12.41	− 0.0177
5.000	1.499	0.992	0.014	13.18	− 0.0241
6.000	1.453	0.968	0.023	13.25	− 0.0321
8.000	1.369	0.953	0.030	13.56	− 0.0382
10.000	1.308	0.939	0.039	13.72	− 0.0467
15.000	1.213	0.928	0.050	14.05	− 0.0564

range is the computer software SRIM (Stopping and Range of Ions in Matter) developed by Ziegler et al. [39] SRIM-2008 version was utilized in that work [40].

3 Results and discussion

This study is related to extensive investigation of nuclear radiation shielding parameters of multi-element metallic glasses whose chemical formulas, codes and densities are given in Table 1. Figure 1 and Table 2 present the change in μ_ρ values depending on photon energy. As indicated in Fig. 1, it was found that with the increment in gamma ray energy at the beginning, μ_ρ declined rapidly and gradually decreased between 0.06 and 0.2 MeV. Initially, this notable reduction in μ_ρ is related to photoelectric absorption, which is probably the main interaction between low energy photons and all metallic glasses. In all metallic glasses, μ_ρ is almost constant beyond 0.02 MeV. Compton scattering and pair production are the main processes at medium and high-energy levels. In addition, μ_ρ values have a sudden increase near 0.07 MeV for MG3 sample. Due to the fact that the possibility of photoelectric absorption occurs, the atomic number varies to Z^{4-5}. Therefore, in the MG3 sample containing Hf, a small peak on the K X-ray absorption edge of Hf (65.33 keV) was seen. Furthermore, the chemical composition of the samples moved the μ_ρ values and, therefore, all samples indicate comparable protection properties. MG3 and MG4 own the highest μ_ρ values, whereas the lowest values of μ_ρ pertain to MG2.

The HVL outcomes of the samples under examination at 0.02–20 MeV photon energies are plotted in Fig. 2. The results showed a relation between the density of and the attenuation ability of the samples. It is seen that low-density MG6 and MG2 samples have high HVL values. Enhancing the density cause lower HVL, which indicates that the high density influences assertively the shielding capacity of the glasses. Furthermore, as photon energy increases, HVL values of the samples begin to differ significantly. While low-energy photons up to 0.1 MeV need shorter distance to lose their energy, the high-energy photons mislay their energy at a longer thickness. While MG3 sample was more successful in stopping photons, MG6 showed the worst performance. In general, it can be concluded that BMGs are capable of protecting high-energy photons.

The Z_{eff} curve as a function of the gamma ray energy for metallic glasses is demonstrated in Fig. 3. It is obvious that MG6 has the lowest Z_{eff} due to elements with low atomic number compared to other samples. MG3 sample significantly outscore from other samples with respect to Z_{eff}. The Z_{eff} values of the studied samples are in the range of 21–46. The N_{el} values obtained using Z_{eff} values are given in Fig. 4. Here, it is noteworthy that N_{el} values change in a different trend from the Z_{eff} curve with photon energy. The metallic glasses with lower atomic weight own higher N_{el} values. MG5 and MG6 have the smallest N_{el} values, whereas MG2 and MG3 have the highest number of electrons per unit mass.

The calculated values of equivalent atomic number (Z_{eq}) for metallic glasses are presented at Table 3. The GP fitting parameters of the EBF of MG2 sample is listed in Table 4 for photon energies of 0.15–15 MeV as an example. Figure 5a–f shows the change of EBF of the samples versus the photon energy at various penetration depths. With some exceptions generally, the EBF has smaller values at low and high energies whereas the higher values of EBF are seen for intermediate energy region. In the low-energy zone, it also showed sudden and high peaks around 0.02 MeV for MG1 and 0.06 MeV for MG3. In the low-energy zone, it showed sudden and high peaks around 0.02 MeV for MG1 and 0.06 MeV for MG3. That could be clarified depending on the partial photon interactions in the energy region. The photoelectric absorption is predominant at low-energy region and gamma photons are entirely absorbed and this could give

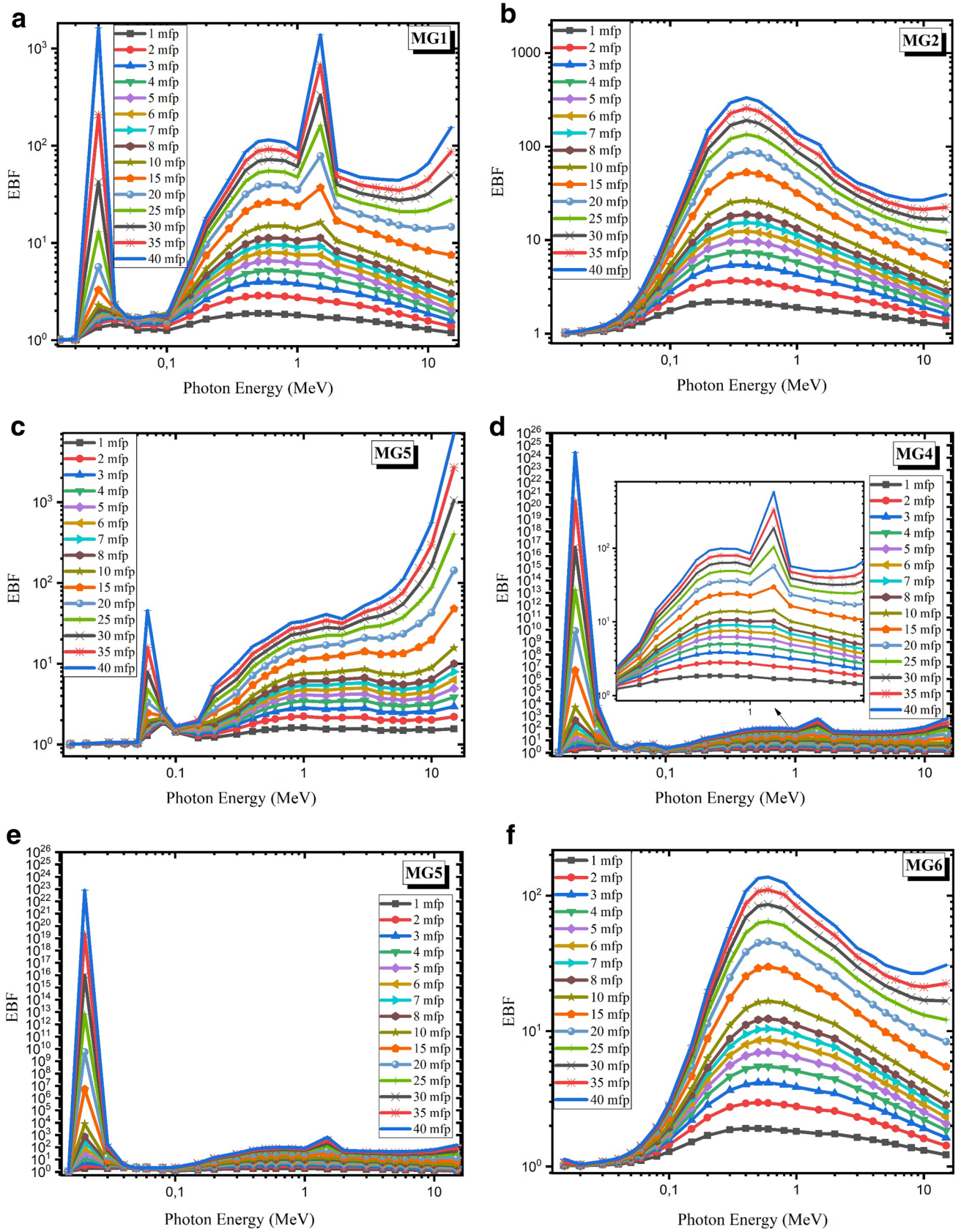

Fig. 5 **a**–**f** EBF at 0.015–15 MeV and 1–40 mfp for the metallic glasses

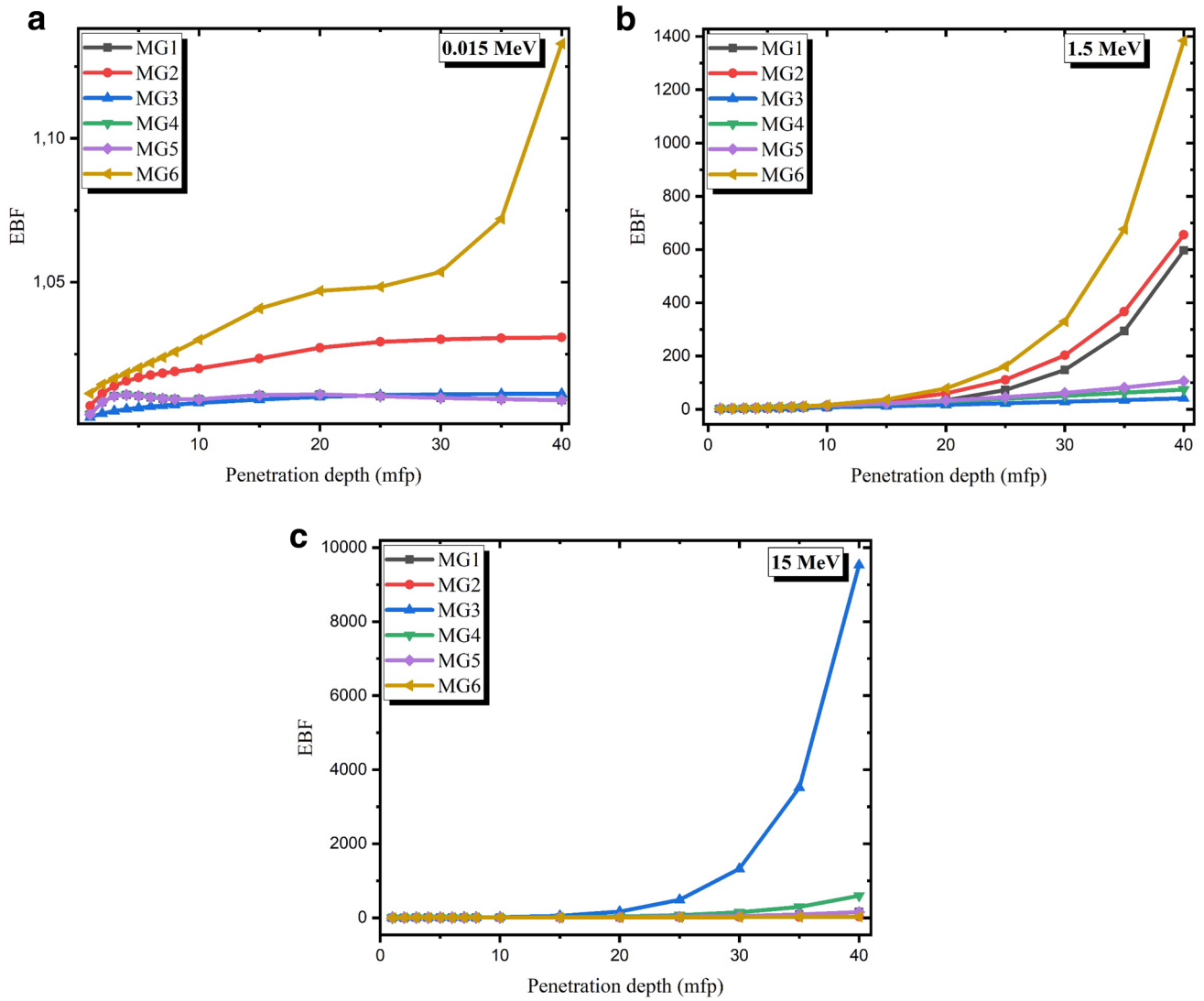

Fig. 6 **a**–**c** The EBF for the glasses up to 40 mfp at 0.015, 1.5, and 15 MeV

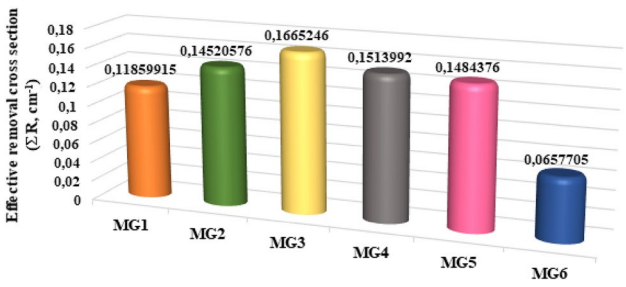

Fig. 7 Effective removal cross-sections of the metallic glasses

rise a very small lifetime to photons which is insufficient for them to buildup in the medium. However, as photoelectric cross-section is proportional with Z^{4-5}, in the case of samples including elements with high atomic numbers, abrupt increments occur near the absorption edge of the element. Therefore, the peaks were seen near the absorption edge of Zr in MG1 (17.99 keV) and Hf (65.35 keV) in MG3. There are sharp peaks at 24.35 keV on the absorption edge of the Pd element contained in MG4 and MG5. Peak intensities were varied depending on the percentage of Pd in the content of the MG4 and MG5 metallic glasses. At medium energies, Compton scattering photons are not fully deducted, but their energy are declined and the probability of photons multiplying in the environment increases. When the increases in the absorption edges are ignored, EBF values are high at middle energies. However, in general the EBF values possess maximum value of around 150 in this region. This is also quite good value for a shielding material. MG3 takes the lower EBF values among the other BMGs at medium energies. Electron–positron pair production happens at 1.022 MeV.

Table 5 Macroscopic effective removal cross-sections of bulk metallic glasses $\sum R$ (cm^{-1})

Element	$\sum R/\rho$ (cm^2/g)	$Ni_{50}Pd_{30}P_{20}$ density = 7.62 g/cm^3		$Pd_{40}Ni_{40}P_{20}$ density = 7.96 g/cm^3	
		Partial density (g cm^{-3})	$\sum R$ (cm^{-1})	Partial density (g cm^{-3})	$\sum R$ (cm^{-1})
P	0.0283	1.5240	0.0431	1.5920	0.0451
Ni	0.0190	3.8100	0.0724	3.1840	0.0605
Pd	0.0144	2.2860	0.0329	3.1840	0.0458
		Total	0.1484		0.1514
		$Ca_{65}Mg_{15}Zn_{20}$ density = 2.69 g/cm^3		$Cu_{49}Hf_{42}Al_9$ density = 10.12 g/cm^3	
Mg	0.0333	0.4035	0.0134		
Ca	0.0243	1.7485	0.0425		
Zn	0.0183	0.5380	0.0098		
Al	0.0293			0.9108	0.0267
Cu	0.0186			4.9588	0.0922
Hf	0.0112			4.2504	0.0476
		Total	0.0657		0.1665
		$Zr_{65}Al_{7.5}Ni_{10}Cu_{17.5}$ density = 6.78 g/cm^3		$Ti_{40}Zr_{26}Be_{28}Fe_6$ density = 4.48 g/cm^3	
Al	0.0293	0.5085	0.0149		
Ni	0.0190	0.6780	0.0129		
Cu	0.0186	1.1865	0.0221		
Zr	0.0156	4.4070	0.0687	1.1648	0.0182
Be	0.0674			1.2544	0.0845
Ti	0.0205			1.7920	0.0367
Fe	0.0214			0.2688	0.0058
		Total	0.1186		0.1452

Therefore, the sudden increments are observed for EBF values of the MG1, MG4 and MG5 at 1 MeV. As the pair production cross-section is proportional to Z^2 at high energies, EBF values increased in metallic glasses with higher Z_{eq} values. As the penetration depth rises, secondary photon formation increases and EBF values start to increase faster.

The variation in EBF values of the BMGs depending on the penetration depth was found for selected fixed energies, 0.015, 1.5 and 15 MeV (Fig. 6a–c). It was obtained that at 0.015 MeV, the EBF values are about 1 and are almost constant with increasing photon energy except MG6. The changes in EBF with the penetration depth at 0.015 and 15 MeV are influenced by the elemental composition of the metallic glasses. At 1.50 MeV, At 1.5 MeV, it is seen that the variation of EBF values increases due to the Z_{eq} values of the samples and became biggest at the large penetration depths. Since at high energies pair production process is the main interactions, EBF is raised with increasing Z_{eq} at 15 MeV for 15–40 mfp. The electron–positron pair and the resulting radiation might leave the sample for low penetration depths. But, when the penetration depth is big, the secondary gamma photons contribute to photon buildup and, therefore, MG3 own the largest EBF values for 15 MeV (Fig. 6c).

The Σ_R outcomes of the studied BMGs are obtained and are demonstrated in Fig. 7 and listed in Table 5. It is clear from Fig. 7 that the Σ_R values are significantly different from each other and changed between 0.065 cm^{-1} for MG6 ($\rho = 2.69$ g/cm^3) and 0.166 cm^{-1} for MG3 ($\rho = 10.12$ g/cm^3). Its higher density than the other metallic glasses clarifies the largest $\sum R$ value for the MG3 sample.

The Stopping and Range of Ions in Materials (SRIM) codes based on Monte Carlo simulation was written to allow the calculation of ion deposition profiles in materials exposed to energetic ion beam [40]. SRIM Monte Carlo code was employed to research proton and alpha mass stopping power (MSP), further proton and alpha projected range (PR) values of selected metallic glasses. The alpha and proton MSP values of metallic glasses against kinetic energy (KE) are presented in Fig. 8a, b. Initially with increasing kinetic energy, MSP values reach maximum. Then, the MSP values decrease as the kinetic energy further increase. As the elements with high atomic number increases in the metallic glasses, MSP values decrease and MG3 sample owns the lowest MSP values of both alpha and proton in the selected kinetic energy range. This result is also related to the high density of MG3 glass. Furthermore, Fig. 9a, b illustrates the variation of projected

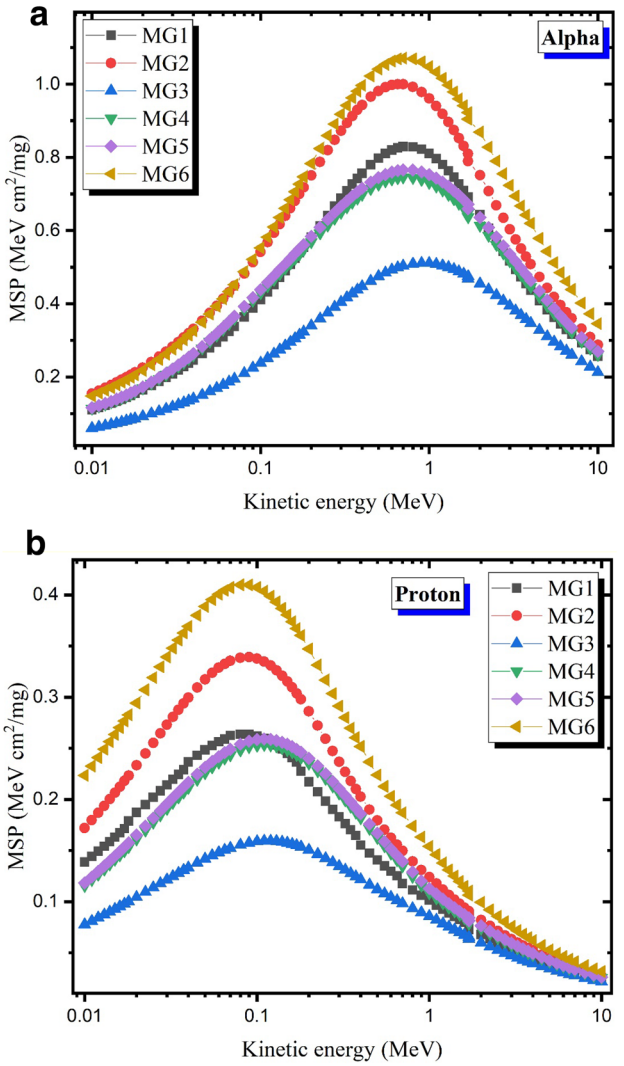

Fig. 8 Alpha and proton mass stopping power (MSP) as a function of kinetic energy for metallic glass samples

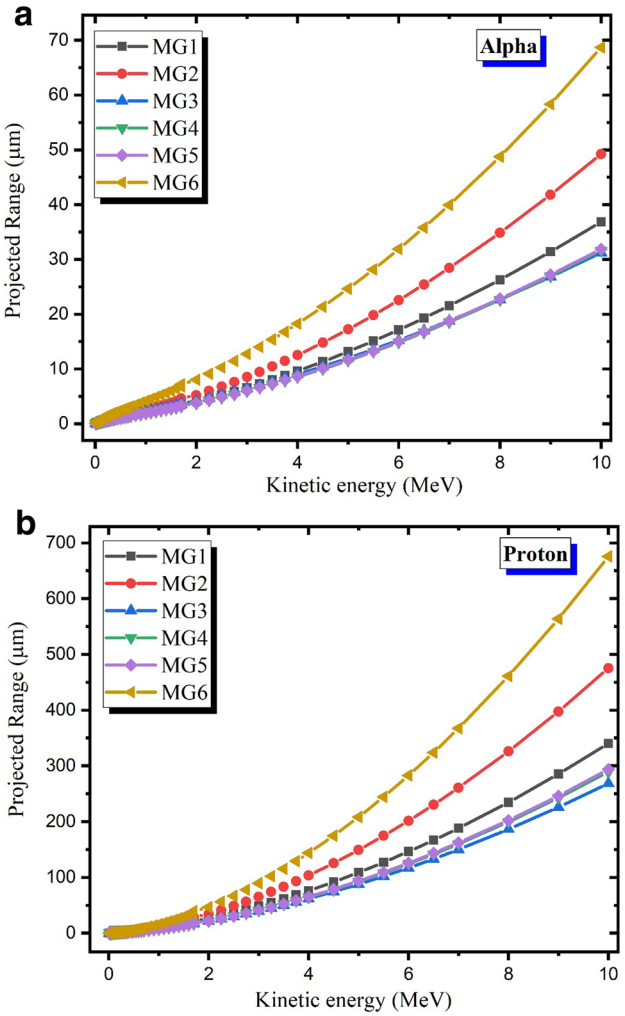

Fig. 9 Alpha and proton projected range (PR) as a function of kinetic energy for metallic glass samples

range (PR), which is another important proton and alpha protection properties, with kinetic energy. For the best alpha and proton protective materials, the lowest PR is required. Therefore, MG3 sample has the lowest PR values. As a result, it can be said that the MG3 is the perfect shield compared to the other samples to be utilized and developed for alpha, proton, gamma and neutron shielding practices.

4 Conclusion

The nuclear shielding calculations of six bulk metallic glasses were acquired in this work. The μ_ρ values of the samples under study were found for 0.020–20 MeV photon energies using WinXCOM program. Besides, the HVL thickness of the metallic glasses was estimated using the linear attenuation coefficients. The outcomes exhibited that MG3 and MG6 samples own the largest and smallest HVL among the selected samples. The highest Z_{eff} values were found to belong to samples containing heavy elements in the composition. In addition, it was concluded that the EBF values of MG3, MG4 and MG5 were lower than those of other samples. The outcomes show that as the Z_{eq} values of the metallic glasses increased, the EBF values decreased and the elements Pd, Hf, and Zr, in the samples prevented the buildup of the photons at medium energies. On the other hand, due to the largest $\sum R$ value of MG3, we can say that it possesses better neutron shielding efficiencies than the others. In addition, it was found that MG3 sample owns the lowest PR and the MSP values among the all of the samples. Taking into account all

these, it can be concluded from this study that metallic glasses have superior shielding performance for gamma, neutral and charged particle radiations. It is seen clearly that selected metallic glasses are promising candidates for nuclear shielding applications as compared with some important shield materials.

References

1. B. Oto, N. Yildiz, T. Korkut, E. Kavaz, Neutron shielding qualities and gamma ray buildup factors of concretes containing limonite ore. Nucl. Eng. Des. (2015). https://doi.org/10.1016/j.nucengdes.2015.07.060
2. I. Akkurt, H. Akyildirim, B. Mavi, S. Kilincarslan, C. Basyigit, Radiation shielding of concrete containing zeolite. Radiat. Meas. (2010). https://doi.org/10.1016/j.radmeas.2010.04.012
3. E.S.A. Waly, M.A. Fusco, M.A. Bourham, Gamma-ray mass attenuation coefficient and half value layer factor of some oxide glass shielding materials. Ann. Nucl. Energy (2016). https://doi.org/10.1016/j.anucene.2016.05.028
4. R. El-Mallawany, M.I. Sayyed, M.G. Dong, Comparative shielding properties of some tellurite glasses: part 2. J. Non-Cryst Solids (2017). https://doi.org/10.1016/j.jnoncrysol.2017.08.011
5. N. Ekinci, E. Kavaz, B. Aygün, U. Perişanoğlu, Gamma ray shielding capabilities of rhenium-based superalloys. Radiat. Eff. Defects Solids **0150**, 1–17 (2019). https://doi.org/10.1080/10420150.2019.1596110
6. N.S. Prabhu, V. Hegde, M.I. Sayyed, O. Agar, S.D. Kamath, Investigations on structural and radiation shielding properties of Er 3+ doped zinc bismuth borate glasses. Mater. Chem. Phys. (2019). https://doi.org/10.1016/j.matchemphys.2019.03.074
7. E. Kavaz, An experimental study on gamma ray shielding features of lithium borate glasses doped with dolomite, hematite and goethite minerals. Radiat. Phys. Chem. (2019). https://doi.org/10.1016/j.radphyschem.2019.03.032
8. E. Kavaz, H.O. Tekin, N.Y. Yorgun, F. Özdemir, M.I. Sayyed, Structural and nuclear radiation shielding properties of bauxite ore doped lithium borate glasses: Experimental and Monte Carlo study. Radiat. Phys. Chem. (2019). https://doi.org/10.1016/j.radphyschem.2019.05.019
9. E. Kavaz, N.Y. Yorgun, Gamma ray buildup factors of lithium borate glasses doped with minerals. J. Alloy Compd. (2018). https://doi.org/10.1016/j.jallcom.2018.04.106
10. M.I.Sayyed, A. Kumar, H.O. Tekin, R. Kaur, M. Singh, O. Agar, M.U. Khandaker, Evaluation of gamma-ray and neutron shielding features of heavy metals doped Bi2O3-BaO-Na2O-MgO-B2O3. Progress Nucl. Energy. (2020). 10.1016/j.pnucene.2019.103118.
11. M.I. Sayyed, K.M. Kaky, M.H.A. Mhareb, A.H. Abdalsalam, N. Almousa, G. Shkoukani, M.A. Bourham, Borate multicomponent of bismuth rich glasses for gamma radiation shielding application. Radiat. Phys. Chem. (2019). https://doi.org/10.1016/j.radphyschem.2019.04.005
12. S.A.M. Issa, A. Kumar, M.I. Sayyed, M.G. Dong, Y. Elmahroug, Mechanical and gamma-ray shielding properties of TeO2-ZnO-NiO glasses. Mater. Chem. Phys. (2018). https://doi.org/10.1016/j.matchemphys.2018.01.058
13. S.A.M. Issa, H.O. Tekin, R. Elsaman, O. Kilicoglu, Y.B. Saddeek, M.I. Sayyed, Radiation shielding and mechanical properties of Al2O3-Na2O-B2O3-Bi2O3 glasses using MCNPX Monte Carlo code. Mater. Chem. Phys. (2019). https://doi.org/10.1016/j.matchemphys.2018.10.064
14. S.A.M. Issa, M. Ahmad, H.O. Tekin, Y.B. Saddeek, M.I. Sayyed, Effect of Bi 2 O 3 content on mechanical and nuclear radiation shielding properties of Bi 2 O 3 -MoO 3 -B 2 O 3 -SiO 2 -Na 2 O-Fe 2 O 3 glass system. Results Phys. (2019). https://doi.org/10.1016/j.rinp.2019.102165
15. C.H. Wang, W.H. Dong, C. Shek, Bulk metallic glasses. Mater. Sci. Eng. R Rep. **44**(23), 45–89 (2004)
16. W. Klement, R.H. Willens, P. Duwez, Non-crystalline structure in solidified Gold-Silicon alloys. Nature (1960). https://doi.org/10.1038/187869b0
17. A. Inoue, H. Yamaguchi, T. Zhang, T. Masumoto, Al-La-Cu amorphous alloys with a wide supercooled liquid region. Mater. Trans. JIM. (1990). https://doi.org/10.2320/matertrans1989.31.104
18. A. Inoue, T. Zhang, T. Masumoto, Zr-Al-Ni Amorphous Alloys with High Glass Transition Temperature and Significant Supercooled Liquid Region. Mater. Trans. JIM. (1990). https://doi.org/10.2320/matertrans1989.31.177
19. A. Inoue, Stabilization of metallic supercooled liquid and bulk amorphous alloys. Acta Mater. (2000). https://doi.org/10.1016/S1359-6454(99)00300-6
20. J. Ketkaew, W. Chen, H. Wang, A. Datye, M. Fan, G. Pereira, U.D. Schwarz, Z. Liu, R. Yamada, W. Dmowski, M.D. Shattuck, C.S. O'Hern, T. Egami, E. Bouchbinder, J. Schroers, Mechanical glass transition revealed by the fracture toughness of metallic glasses. Nat. Commun. (2018). https://doi.org/10.1038/s41467-018-05682-8
21. C.A. Schuh, T.C. Hufnagel, U. Ramamurty, Mechanical behavior of amorphous alloys. Acta Mater. (2007). https://doi.org/10.1016/j.actamat.2007.01.052
22. J. Qiao, H. Jia, P.K. Liaw, Metallic glass matrix composites. Mater. Sci. Eng. R Rep. (2016). https://doi.org/10.1016/j.mser.2015.12.001
23. A. Khmich, K. Sbiaai, A. Hasnaoui, Structural behavior of Tantalum monatomic metallic glass. J. Non-Cryst. Solids (2019). https://doi.org/10.1016/j.jnoncrysol.2019.01.024
24. A. Takeuchi, A. Inoue, Classification of bulk metallic glasses by atomic size difference, heat of mixing and period of constituent elements and its application to characterization of the main alloying element. Mater. Trans. (2005). https://doi.org/10.2320/matertrans.46.2817
25. A. Inoue, High strength bulk amorphous alloys with low critical cooling rates (Overview). Mater. Trans. JIM. (1995). https://doi.org/10.2320/matertrans1989.36.866
26. A. Inoue, Bulk glassy alloys: historical development and current research. Engineering. (2015). https://doi.org/10.15302/J-ENG-2015038
27. M. Chen, Mechanical behavior of metallic glasses: microscopic understanding of strength and ductility. Annu. Rev. Mater. Res. (2008). https://doi.org/10.1146/annurev.matsci.38.060407.130226
28. K.A. Avchaciov, Y. Ritter, F. Djurabekova, K. Nordlund, K. Albe, Controlled softening of Cu64Zr36 metallic glass by ion irradiation. Appl. Phys. Lett. (2013). https://doi.org/10.1063/1.4804630
29. Y.H. Qiu, C. Xu, E.G. Fu, P.P. Wang, J.L. Du, Z.Y. Hu, X.Q. Yan, X.Z. Cao, Y.G. Wang, L. Shao, Mechanisms for the free volume tuning the mechanical properties of metallic glass through ion irradiation. Intermetallics (2018). https://doi.org/10.1016/j.intermet.2018.08.006
30. S.A.M. Issa, T.A. Hamdalla, A.A.A. Darwish, Effect of ErCl3in gamma and neutron parameters for different concentration

of ErCl3-SiO2(EDFA) for the signal protection from nuclear radiation. J Alloy Compd. (2017). https://doi.org/10.1016/j.jallcom.2016.12.176
31. E. Kavaz, U. Perişanoğlu, N. Ekinci, Y. Özdemır, Determination of energy absorption and exposure buildup factors by using G-P fitting approximation for radioprotective agents. Int. J. Radiat. Biol. (2016). https://doi.org/10.1080/09553002.2016.1175681
32. L. Gerward, N. Guilbert, K.B. Jensen, H. Levring, WinXCom—a program for calculating X-ray attenuation coefficients. Radiat. Phys. Chem. (2004). https://doi.org/10.1016/j.radphyschem.2004.04.040
33. O. Agar, E. Kavaz, E.E. Altunsoy, O. Kilicoglu, H.O. Tekin, M.I. Sayyed, T.T. Erguzel, N. Tarhan, Er 2 O 3 effects on photon and neutron shielding properties of TeO 2 -Li 2 O-ZnO-Nb 2 O 5 glass system. Results Phys. (2019). https://doi.org/10.1016/j.rinp.2019.102277
34. J.M. Sharaf, H. Saleh, Gamma-ray energy buildup factor calculations and shielding effects of some Jordanian building structures. Radiat. Phys. Chem. (2015). https://doi.org/10.1016/j.radphyschem.2015.01.031
35. B. Oto, S.E. Gulebaglan, Z. Madak, E. Kavaz, Effective atomic numbers, electron densities and gamma rays buildup factors of inorganic metal halide cubic perovskites CsBX3 (B = Sn, Ge; X = I, Br, Cl). Radiat. Phys. Chem. **159**, 195–206 (2019). https://doi.org/10.1016/j.radphyschem.2019.03.010
36. K.S. Mann, J. Singla, V. Kumar, G.S. Sidhu, Investigations of mass attenuation coefficients and exposure buildup factors of some low-Z building materials. Ann. Nucl. Energy (2012). https://doi.org/10.1016/j.anucene.2012.01.004
37. K.S. Mann, T. Korkut, Gamma-ray buildup factors study for deep penetration in some silicates. Ann. Nucl. Energy (2013). https://doi.org/10.1016/j.anucene.2012.08.024
38. E. Kavaz, N. Ekinci, H.O. Tekin, M.I. Sayyed, B. Aygün, U. Perişanoğlu, Estimation of gamma radiation shielding qualification of newly developed glasses by using WinXCOM and MCNPX code. Prog. Nucl. Energy **115**, 12–20 (2019). https://doi.org/10.1016/j.pnucene.2019.03.029
39. J.F. Ziegler, SRIM-2003, In: Nuclear ınstruments and methods in physics research, section B: beam ınteractions with materials and atoms (2004) doi:10.1016/j.nimb.2004.01.208.
40. F. James, J.F. Ziegler, J.P. Biersack, M.D. Ziegler, SRIM, the stopping and range of ions in matter. Nucl. Instrum. Methods Physics Res. B. (2008). https://doi.org/10.1016/j.nimb.2004.01.208.4